

APPLICATION OF THE SPH METHOD TO COMPRESSION OF SOLID MATERIALS

Gerald G. PEREIRA*, Paul W. CLEARY and Vincent LEMIALE

CSIRO Digital Productivity Flagship, Clayton, Victoria 3169, AUSTRALIA

*Corresponding author, E-mail address: Gerald.Pereira@csiro.au

ABSTRACT

Smoothed Particle Hydrodynamics (SPH) is a numerical method that does not use a mesh or grid when solving a set of partial differential equations. This makes it particularly useful in application to solid mechanics problems where the sample undergoes large deformation. Whereas mesh-based methods have difficulty when the sample becomes severely distorted, SPH naturally deals with this important engineering scenario. We implement the SPH method for compressional deformation of solid samples and focus on uniaxial, biaxial and triaxial loading. We develop a numerical procedure that naturally deals with these three different sets of boundary conditions and apply it to both small and larger strains in elastic and more complex materials.

NOMENCLATURE

r	position
v	velocity
m	mass
P	pressure
g	body force
S	deviatoric stress tensor
G	shear modulus
K	bulk modulus
c	speed of sound
ρ	density
ϵ	strain tensor
Ω	rotation tensor
σ	(total) stress tensor
σ_{VM}	von Mises stress
Π	artificial viscous stress tensor
Ψ	colour function

Superscripts/subscripts

i, j	superscript indicating tensor components
a, b	subscripts indicating SPH particles

INTRODUCTION

Compressional tests of solid materials are used extensively to determine mechanical properties and to characterize solid material behaviour. Three main types of compressional tests are usually implemented – *uniaxial*, *biaxial* and *triaxial* tests. The usual shape of the sample is a cylinder or a rectangular block (cuboid). In uniaxial tests this solid sample is placed between flat plates (platens). Grips may also be placed on the sample ends to prevent slippage on the platens. One end of the sample is pushed

by a moving piston, at a uniform rate or by a given force, while the other end is fixed. Using suitable sensors (strain gauge or extensometers) mechanical properties of the sample can be determined for the test. Biaxial tests are carried out on cuboid samples. This test is set up similarly to a uniaxial test but with the additional condition that on a pair of opposite free faces a compressive normal stress is applied. Finally, a triaxial test can be performed on either cylinders or cuboids, but here a normal stress is placed on all remaining free surfaces. Usually this can be done by immersing the sample in a fluid (such as oil) at high pressure.

Numerical modelling of these compressional tests have been reported on (for various numerical methods). However our main emphasis in this paper is to model these tests to high strain in the sample. This means the sample may deform in shape. Traditional numerical techniques such as finite element or finite volume methods implement a mesh to cover the volume domain of the material. When the sample deforms significantly these mesh methods can become inaccurate. Alternatively re-meshing the constantly deforming irregular domain can be problematic with high cost and numerical diffusion.

A computational method which does not use a mesh would be ideal for this problem. Smoothed Particle Hydrodynamics (SPH) is a meshless computational method which can be used for solving sets of partial differential equations. It was originally proposed by Gingold and Monaghan (1977) and independently by Lucy (1977) for application to astrophysical problems. It has since been applied extensively for solving the Navier-Stokes equations in a diverse range of applications (Cleary et al, 2002, Pereira et al, 2012, Tartakovsky et al 2015, Kajtar & Monaghan, 2012). For a comprehensive review of these applications see Monaghan (2012). More recently it has begun to be applied to solid mechanical problems (Libersky and Petschek, 1990, Gray et al, 2001, Bui et al, 2008 and Lemaile et al, 2014). Very recently Das and Cleary (2015) applied the SPH method to model uniaxial compression of solid samples for infinitesimal deformation. Their main aim was to compare the stability, convergence and accuracy of SPH to finite element solutions for the stress wave propagation through the sample. They found that the SPH method was well suited to accurately model elastic solids that are subject to uniaxial compression.

The mesh-free nature of SPH means that it can be used for problems with very large strains – well above those where grid or mesh based methods fail due to mesh distortion

and avoids any requirements of adaptive re-meshing and the associated numerical diffusion from the grid to grid interpolation. Specifically SPH is attractive for modelling of large strain deformation of continuous rock masses and so may be applied to geological and geomechanical problems.

As mentioned above the only previously published work on applications of SPH to solid compressional tests has been to infinitesimal deformation of uniaxial tests (Das and Cleary, 2015). In this paper, we are therefore motivated to apply the SPH method to much larger deformation of the sample. In addition, we would like to encompass a larger range of common mechanical tests. These are the biaxial and triaxial tests. In both these cases a normal stress is placed on the sides of the sample. In the biaxial test, as described above, an opposite pair of parallel sides are subject to a normal stress leaving the sample to deform freely in the remaining direction. This is therefore a fully three-dimensional problem. In the triaxial test, normal stresses are placed on all remaining sides (of the cylinder or cuboid). As the sample deforms, one must also track the deforming sides, so as to apply the normal stress.

In the following we describe the SPH method for solids and focus on application of the boundary conditions for the various mechanical tests. We then apply these new boundary conditions to uniaxial, biaxial and triaxial compressions and consider large deformation of the samples.

SMOOTHED PARTICLE HYDRODYNAMICS APPLIED TO SOLID MATERIALS

The application of SPH to the modelling of solid elastic materials is well established. Here we give a brief overview of the method and then focus on the new treatment of biaxial and triaxial boundary conditions.

The SPH continuity equation, taken from Monaghan (1992), is:

$$\frac{d\rho_a}{dt} = \sum_b m_b (\mathbf{v}_a - \mathbf{v}_b) \cdot \nabla W_{ab} \quad (1)$$

where m_b is the mass of particle b , ρ_a is the density of particle a with velocity \mathbf{v}_a . Here $W(\mathbf{r}, h)$ is a C^2 spline based interpolation or smoothing kernel with radius $2h$ that approximates the shape of a Gaussian function. We denote the position vector from particle b to particle a by $\mathbf{r}_{ab} = \mathbf{r}_a - \mathbf{r}_b$ and let $W_{ab} = W(\mathbf{r}_{ab}, h)$ be the interpolation kernel with smoothing length h evaluated at distance $|\mathbf{r}_{ab}|$. This form of the continuity equation is Galilean invariant (since the positions and velocities appear only as differences), has good numerical conservation properties and is not affected by free surfaces or density discontinuities.

The momentum equation used for predicting elastic deformation of solids is:

$$\frac{d\mathbf{v}}{dt} = \frac{1}{\rho} \nabla \cdot \boldsymbol{\sigma} + \mathbf{g} \quad (2)$$

where \mathbf{v} is the velocity, \mathbf{g} is a body force such as gravity and $\boldsymbol{\sigma}$ is the stress tensor which is written as $\boldsymbol{\sigma} = -P\mathbf{I} + \mathbf{S}$.

Here P is the isotropic pressure and \mathbf{S} is the deviatoric stress, while \mathbf{I} is the identity tensor. Assuming Hooke's Law with shear modulus G , the evolution equation for the deviatoric stress \mathbf{S} is calculated using the Jaumann rate equation (Gray et al, 2001)

$$\frac{d\mathbf{S}^{ij}}{dt} = 2G \left(\dot{\varepsilon}^{ij} - \frac{1}{3} \delta^{ij} \dot{\varepsilon}^{kk} \right) + \mathbf{S}^{ik} \boldsymbol{\Omega}^{kj} + \boldsymbol{\Omega}^{ik} \mathbf{S}^{kj} \quad , \quad (3)$$

where the components of the rate of strain tensor $\dot{\varepsilon}$ are given by

$$\dot{\varepsilon}^{ij} = \frac{1}{2} \left(\frac{dv^i}{dx^j} + \frac{dv^j}{dx^i} \right) \quad (4)$$

and the rotation tensor $\boldsymbol{\Omega}$ that accounts for the large rotational effect is given by

$$\boldsymbol{\Omega}^{ij} = \frac{1}{2} \left(\frac{dv^i}{dx^j} - \frac{dv^j}{dx^i} \right) \quad . \quad (5)$$

The SPH discretisation of the momentum equations (2) and (3) is

$$\frac{d\mathbf{v}_a}{dt} = \sum_b m_b \left(\frac{\boldsymbol{\sigma}_a}{\rho_a} + \frac{\boldsymbol{\sigma}_b}{\rho_b} + \Pi_{ab} \mathbf{I} \right) \cdot \nabla_a W_{ab} + \mathbf{g} \quad . \quad (6)$$

Here $\boldsymbol{\sigma}_a$ and $\boldsymbol{\sigma}_b$ are the stress tensors of particles a and b , and Π_{ab} is an artificial viscous stress term that produces shear and bulk viscosities. For particle a , the SPH equations for the components of the strain rate $\dot{\varepsilon}_a$ and the rotation tensor $\boldsymbol{\Omega}_a$ are:

$$\dot{\varepsilon}_a^{ij} = \frac{1}{2} \sum_b \frac{m_b}{\rho_b} \left((v_b^j - v_a^j) \frac{\partial W_{ab}}{\partial x_a^i} + (v_b^i - v_a^i) \frac{\partial W_{ab}}{\partial x_a^j} \right) \quad (7)$$

$$\boldsymbol{\Omega}_a^{ij} = \frac{1}{2} \sum_b \frac{m_b}{\rho_b} \left((v_b^i - v_a^i) \frac{\partial W_{ab}}{\partial x_a^j} - (v_b^j - v_a^j) \frac{\partial W_{ab}}{\partial x_a^i} \right) \quad . \quad (8)$$

The artificial viscous stress in (6) enhances solution stability. For elastic solids, the form of this term (Monaghan and Gingold, 1983) is

$$\Pi_{ab} = \begin{cases} \frac{-\alpha c \eta_{ab} + \beta \eta_{ab}^2}{\bar{\rho}_{ab}} & \text{if } (\mathbf{v}_a - \mathbf{v}_b) \cdot (\mathbf{r}_a - \mathbf{r}_b) < 0 \\ 0 & \text{if } (\mathbf{v}_a - \mathbf{v}_b) \cdot (\mathbf{r}_a - \mathbf{r}_b) \geq 0 \end{cases} \quad (9)$$

where

$$\eta_{ab} = \frac{h(\mathbf{v}_a - \mathbf{v}_b) \cdot (\mathbf{r}_a - \mathbf{r}_b)}{|\mathbf{r}_a - \mathbf{r}_b|^2} \quad \text{and} \quad \bar{\rho}_{ab} = \frac{\rho_a + \rho_b}{2} \quad . \quad (10)$$

Here α is the coefficient of the linear term which produces a shear and bulk viscosity and β is the coefficient of the quadratic term which is approximately equal to the Von Neumann-Richmyer viscosity. We use the traditional value of $\alpha = 1.0$ and $\beta = 2.0$.

We use an equation of state where the elastic pressure is proportional to the change in density $P = c^2(\rho - \rho_0)$ where ρ_0 is the reference density, ρ is the current density and c is the speed of sound in the solid material. The sound speed is calculated from the material bulk modulus, K , i.e. $c = \sqrt{K / \rho_0}$, which is the real speed of sound in the material. An improved Euler explicit

integration scheme is used with a time step Δt determined by the Courant condition $\Delta t_s = \min\{0.5h/c_a\}$.

Boundary Conditions

Uniaxial boundary conditions

The boundary conditions for uniaxial compression are prescribed velocities on the top and bottom platens. If we orient the sample so that the compressional direction is parallel to the z -axis, then this implies on the first and last set of SPH particles (in the z -direction) we impose given z -direction speeds. In fact we use a layer of four particles for each platen, so as to avoid issues of incorrect normalisation near the boundary of the dynamic SPH particles. In uniaxial compression, the side boundaries (in x and y directions) are free to deform according to the equation of motion. Because the SPH formulation naturally deals with this, nothing additional has to be applied to these side boundary SPH particles.

Biaxial boundary conditions

In biaxial compression one only uses cuboid samples. This means all faces of the cuboid are planar and parallel to one of the principal axes. The faces perpendicular to the z -axis (compression direction) are treated similarly to the uniaxial case, above. A pair of parallel opposite faces (in this case the faces perpendicular to the x -axis) has a normal stress applied to them, while the remaining two faces (perpendicular to the y -axis) are free to deform (as in the uniaxial case). To apply the normal stress boundary condition to a planar surface we use rigid mesh objects. Each small portion of the mesh imparts a normal force to the SPH particles that are adjacent to it.

Triaxial boundary conditions

Triaxial compression tests are usually carried out with the solid sample being placed in a high pressure fluid. The top and bottom platens are still given prescribed speeds (as in the uniaxial and biaxial cases) but the sides surfaces (whether they be planar, curved or more irregular) have a normal stress applied. So in this case we need to identify the (side) surface boundary particles and a normal force must be applied to them. To do this we need to not only determine which particles are the surface particles but also determine the normal vector to these particles (noting that this can change with large amplitude deformations of the sample).

This is essentially a surface identification problem and similar to the identification of a surface between two immiscible fluids for fluid flow problems. We first define the volume corresponding to the dynamic SPH particle domain, given by:

$$\Psi(\mathbf{r}) = \begin{cases} 1 & \mathbf{r} \in \Xi_m \\ 0 & \mathbf{r} \notin \Xi_m \end{cases}, \quad (11)$$

where Ξ_m is the SPH particle (material) domain. The normal to a surface can be calculated in SPH as follows. Given the function which represents a surface in three-dimensions $\Psi(x,y,z)$, the normal to the surface is easily calculated from its gradient $\nabla\Psi$. In SPH, numerical values of functions and their derivatives are calculated through an interpolation function. For example, the

interpolation of any function Ψ at any position \mathbf{r} using SPH smoothing is given by:

$$\Psi(\mathbf{r}) = \sum_b m_b \frac{\Psi_b}{\rho_b} W(\mathbf{r} - \mathbf{r}_b, h). \quad (12)$$

The gradient of the function Ψ is given by differentiating the interpolation equation (12) to give:

$$\nabla\Psi(\mathbf{r}) = \sum_b m_b \frac{\Psi_b}{\rho_b} \nabla W(\mathbf{r} - \mathbf{r}_b, h). \quad (13)$$

The problem with using equation (13) for calculating gradients is that it produces noisy estimates. A numerically better (less noisy) estimate of the gradient is the symmetric expression

$$\frac{\rho_a}{m_a} \nabla\Psi(\mathbf{r}) = \sum_b \left(\frac{\Psi_b}{(m_b/\rho_b)^2} + \frac{\Psi_a}{(m_a/\rho_a)^2} \right) \nabla W(\mathbf{r} - \mathbf{r}_b, h). \quad (14)$$

The important point to note here is that interior particles, when suitably averaged, will yield comparatively small (magnitude) normals. On the other hand surface particles will have a sizeable (non-zero) normal. A criterion is therefore implemented to ignore particles with normal magnitudes below a certain threshold. The unit normal, $\underline{\mathbf{n}}$ to the surface is calculated from equation (14), for those particles satisfying the threshold criterion, after being suitably normalised.

To model the triaxial boundary conditions, for all surface particles (those identified as having a non-negligible normal) we add an additional normal force, \mathbf{F} :

$$\mathbf{F} = -P_{\text{triaxial}} \Delta^2 \underline{\mathbf{n}}, \quad (15)$$

where P_{triaxial} is the fluid pressure, Δ is the SPH particle separation and the negative sign indicates the force is into the sample.

In our results we display the von Mises stress field during compression. The von Mises yield criterion is commonly used in engineering applications to assess the failure strength of a material. The von Mises stress, σ_{VM} , is given by

$$\sigma_{\text{VM}} = \sqrt{\frac{(\sigma_1 - \sigma_2)^2 + (\sigma_2 - \sigma_3)^2 + (\sigma_1 - \sigma_3)^2}{2}}. \quad (16)$$

Here σ_1 , σ_2 and σ_3 are the three principal stresses.

RESULTS

Previous SPH modelling of uniaxial and triaxial compression tests were reported by Das and Cleary (2015, 2008). Initially, we validate against those results by comparing the early time stress wave propagation for the two cases in three-dimensional cuboid samples. Figure 1 shows the stress wave propagation for uniaxial and triaxial compression taken at 0.36 ms. Material properties of the sample are bulk modulus of 7.47 GPa, shear modulus of 2.67 GPa and density of 2300kg/m³ to give a sound speed of 1802 m/s. The cuboid sample has dimensions 8.6 cm x

8.6 cm x 14 cm and we use an SPH particle spacing of 3 mm with a total of around 40,000 SPH particles. The upper piston surface moves down at 1.5 mm/s. The uniaxial compression stress wave travels downwards before reflecting off the bottom surface. The triaxial compression test imposes a uniform normal pressure of 70 MPa on the sides of the cuboid. In this case the stress waves are initiated from not only the top but also the four sides. These waves collide near the centre of the sample generating a more complex stress pattern. Due to the pressure from the sides, the magnitude of the von Mises stress is significantly larger in the triaxial case (by a factor of approximately three) compared to the uniaxial case. The early stage evolution of the stress wave pattern thus agrees generally with previous studies (Das & Cleary, 2008, 2015).

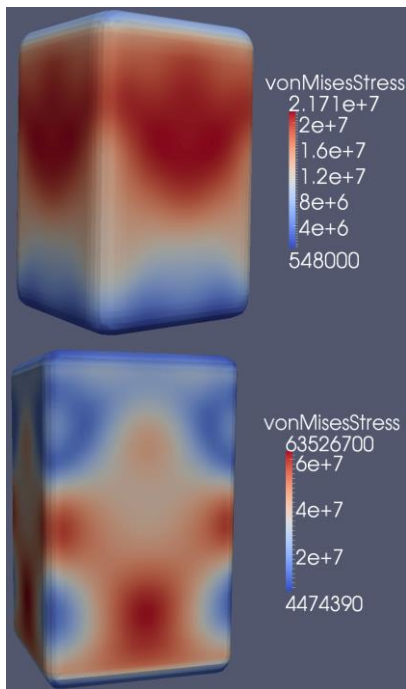


Figure 1: Stress wave during uniaxial (above) and triaxial (below) compression for cuboid samples. Colour bar has units of Pa. See text for material properties and other quantities used in simulation.

Biaxial test

SPH simulations of three-dimensional biaxial tests have not been reported on before. So now we consider this case with the same material properties and sample size (as above) but with a normal pressure of 70 MPa only on the side walls perpendicular to the x -axis. Figure 2 shows the early stage stress wave pattern. One can see the lateral pressure generates the main stress in the sample at this early stage. High stress regions are close to the two side walls. As time progresses the waves travel inwards and interfere near the sample centre. In the third (free direction) there is no significant stress variation at this stage but over time the strain is allowed to relax in this direction which is an important aspect of the biaxial test.

Curved boundaries

The previous SPH compression studies dealt with cuboid samples. We now consider samples with curved side boundaries, which are a main focus of this paper.

We consider a cylindrical sample, with otherwise similar conditions to those outlined for the cuboid sample of Fig. 1 except we used a uniform normal pressure of 20 MPa for the triaxial test. Larger normal pressures tend to cause rotation of the sample between the platens, most probably caused by slippage between the sample and platens. Figure 3 shows the stress wave profiles for the two cases. In the uniaxial case stress waves are created from the top (as before) and travel down the sample before reflecting. In contrast to the cuboid case, because the sample does not have the long edges, the stress wave pattern does not have the typical V-shape but is planar. In contrast, because of the uniform normal pressure, the triaxial compression (Fig. 3b) stress wave pattern displays axial high and low stress regions. These axial bands appear almost immediately and persist to steady state. Once again, as in the cuboid case, the magnitude of the von Mises stress is much larger in the triaxial test than the uniaxial test (by roughly a factor of three).

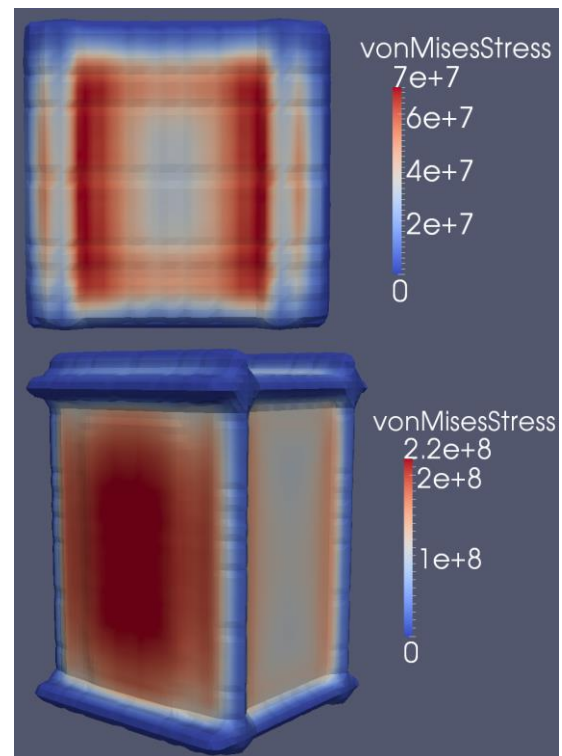


Figure 2: Stress wave pattern for a biaxial compression test. View from above the platen (above) and side-on (below). Colour bar has units of Pa.

We now consider a curved shape for the sample (a cylinder) and extend the tests to much larger times, so as to study large deformation of the sample. This situation is of significance in engineering applications. For this case we use a density and moduli approximating rubber, i.e. density of 1000 kg/m^3 , bulk modulus of 1 GPa and shear modulus of 0.6 MPa. The result of this compression at about 3% strain is shown in Fig. 4. The uniaxial compression shows mainly lateral stress variations while the triaxial compression shows both lateral and axial variation which are generated from the lateral pressures. The uniaxial simulation was run to 5 seconds and showed an observable sample deformation. It tended to bulge near the centre of the sample (equidistant from each platen).

However, larger deformation in the triaxial simulation was limited by lateral movement of the sample between the platens after about 2 seconds, caused by slippage between sample and platens. Limiting this slippage will be addressed in future work.

More complex constitutive models

The elastic model presented in equations (3) and (4) has a limited range of applicability. Many materials show much more complex rheological and deformation behaviour, particularly involving different amounts and types of plasticity. As a consequence the shape of the sample may vary in a more complex manner. It is useful to also determine how this SPH method deals with these more complex models in different compressive loading conditions.

For this test we attempt to model a rock sample which has an elasto-plastic response, with a softer material in the middle of the sample and harder material near the platens. We use a Drucker-Prager model (Bui et al, 2008, Lemaile et al, 2014) with the application of this model to direct shear tests being recently reported in Cleary et al (2015). The materials both have density 2380 kg/m^3 . The harder material has a bulk modulus 20 GPa and shear modulus 0.23 GPa. The softer material has bulk modulus 10 GPa and shear modulus 0.2 GPa. To model the solid materials the Drucker-Prager model is implemented with plain strain conditions and the following values for the parameters yield stress/cohesion, friction angle and dilatancy angle: 20 MPa, 24.7 and 10.0 for the harder material and 8 MPa, 46.1 and 10.0 for the softer material.

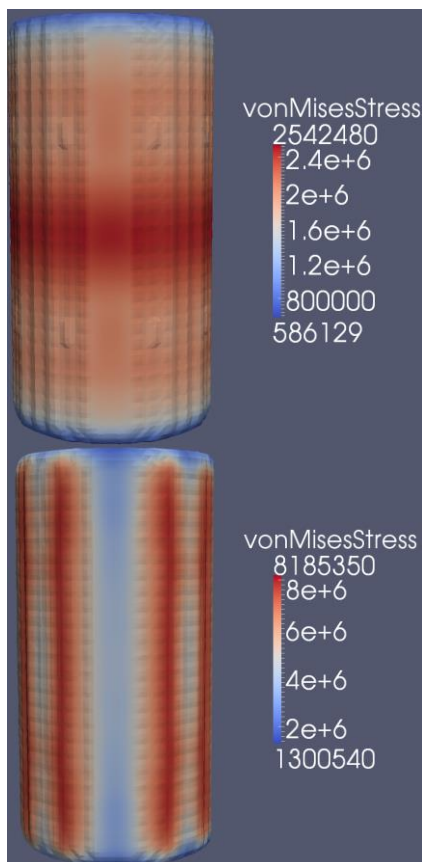


Figure 3: Stress wave pattern for a uniaxial (above) and triaxial (below) compression on a cylindrical sample. Colour bar has units of Pa.

Figure 5 shows samples at 30% strain for both uniaxial and triaxial compression with a normal pressure of 40MPa. Firstly the uniaxial sample develops a curved boundary in the axial direction with a bulge in the sample around the middle plane. The sample diameter increases (from platens to the midpoint) by a factor of 1.4 while the overall shape of the sample remains comparatively symmetric. The maximum von Mises stress is around 45 MPa, near where the platens and sample meet. On the other hand, triaxial compression does not show any significant bowing (curvature) in the axial direction. The cylindrical boundaries remain quite straight with the sample expanding uniformly in the radial direction at all heights. By volume conservation the radius has now increased by a factor of 1.19 from its initial value. So the applied normal pressure appears to have prevented sample bulging, as one may expect intuitively. The maximum von Mises stress in the sample, for the triaxial case, is about double the uniaxial case at 80 MPa and this appears to be quite uniform throughout the sample. It should be noted that beyond this point, the sample began to slide sideways between the platens, due to the high stresses it was experiencing and the absence of platen friction in the model.

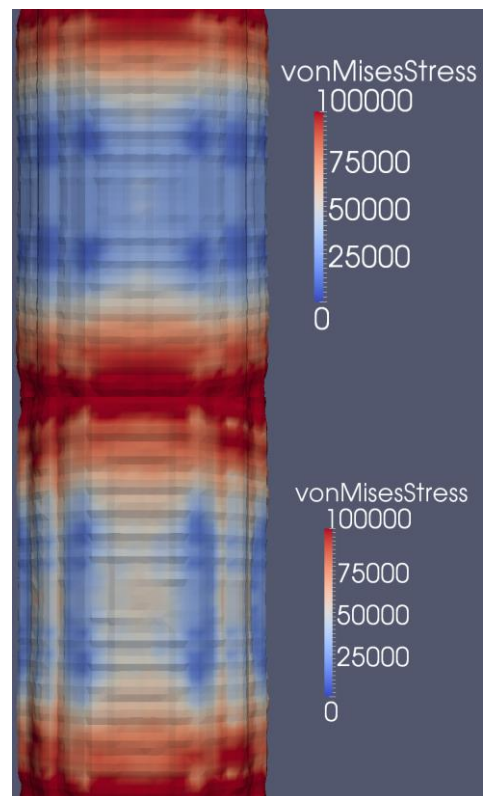


Figure 4: Von Mises stress for a rubber sample at around 3% strain for uniaxial compression (above) and triaxial compression (below). Colour bar has units of Pa.

CONCLUSION

In this paper we have introduced a method to model confined boundary conditions when solid samples undergo compression. In principle, this method will also work for

samples under tension. The three situations we have focussed on are uniaxial, biaxial and triaxial compression. Biaxial compression is a special case which only deals with cuboid samples but the other two cases can deal with any regular shaped sample (such as cuboids, cylinders etc). The case of uniaxial compression is naturally dealt with in the SPH methodology as SPH particles can move (and hence the sample deform) in response to a given force. This is an appealing feature of SPH as can be clearly see in Fig. 5.

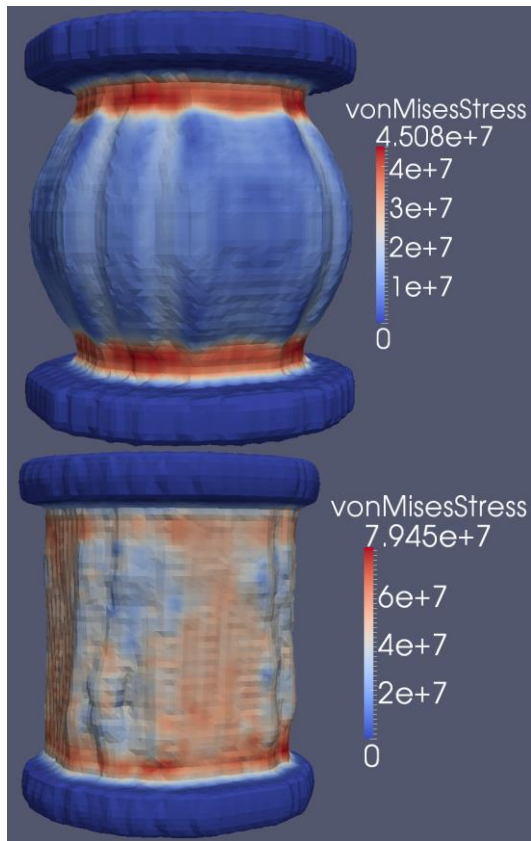


Figure 5: Von Mises stress and sample deformation for uniaxial (above) and triaxial (below) compression on an initial cylindrical sample with a Drucker-Prager model. Both cases are shown at 30% strain. Colour bar has units of Pa.

Biaxial boundary conditions have been tried and tested at relatively low strain. The stress wave pattern shows qualitatively correct behaviour, but future work will consider this at a quantitative level. Triaxial boundary conditions have been applied on cuboid samples as well as cylindrical samples. Once again they appeared to give qualitatively correct behaviour. Comparison with theory is difficult here as there are no available analytical models and comparison with other numerical models is problematic at high strain. However we can say whenever a lateral pressure is applied to a sample the overall von Mises stress in the sample increases. Full stress-strain curves (to compare with experiments) will be given in a future publication.

There are some numerical problems which need consideration. Our biaxial simulations at high strain have issues which we are presently working on. Some triaxial simulations show both rotation and sideways movement of

the sample between the platens. These effects are related to slipping of the sample between platens. In reality, friction is present which prevents the sample slipping on the platens. This is presently being considered in our modelling and will be reported on in the near future.

REFERENCES

- BUI, H. H., FUKAGAWA, R., SAKO, K., and OHNO, S., (2008), "Lagrangian meshfree particles method (SPH) for large deformation and failure flows of geomaterial using elastic-plastic soil constitutive model", *Int. J. Numer. Anal. Met.*, **32**, 1537–1570.
- CLEARY, P.W., HA, J., ALGUINE, V. and NGUYEN, T., (2002), "Simulation of casting complex shaped objects using SPH", *Appl. Math. Model.*, **26**, 171-190.
- CLEARY, P.W., PEREIRA, G.G. LEMAILE, V., DELLE PIANE, C and CLENNELL, B., (2015), "Multiscale model for predicting shear zone structure and permeability in deforming rock", submitted to *Computational Particle Mechanics*.
- DAS, R. and CLEARY, P.W., (2015), "Evaluation of the accuracy and stability of the classical SPH method under uniaxial compression", *J. Scientific Computing*, (in press).
- DAS, R. and CLEARY, P.W., (2008), "Triaxial compression test modelling using SPH", CSIRO Technical report, Melbourne Australia, Report # CMIS-06/121.
- GINGOLD, R.A. and MONAGHAN, J.J., (1977), "Smoothed particle hydrodynamics – Theory and application to non-spherical stars", *MNRAS*, **181**, 375-389.
- GRAY, J.P., MONAGHAN, J.J. and SWIFT, R.P. (2001), "SPH elastic dynamics", *Comp. Meth. Appl. Mech. and Eng.*, **190**, 6641-6662.
- KAJTAR, J.B., and MONAGHAN, J.J., (2012) "On the swimming of fish like bodies near free and fixed boundaries", *Eur. J. Mech. B – Fluids*, **33**, 1-13.
- LEMAILE, V., KARANTGIS, L., and BROADBRIDGE, P., (2014), "Smoothed Particle Hydrodynamics applied to the modelling of landslides", *Appl. Mech. Mat.*, **553**, 519-524.
- LIBERSKY, L.D. and PETSCHKE, A.G., "Smoothed Particle Hydrodynamics with strength of materials", (1990), In "*Advances in the free Lagrangian method*", ed Trease and Crowley, Berlin; Springer.
- LUCY, L.B., (1977), "A numerical approach to the testing of the fission hypothesis", *Astron. J.*, **83**, 1013-1024.
- MONAGHAN, J. J., (1992), "Smoothed particle hydrodynamics", *Ann. Rev. Astron. Astrophys.*, **30**, 543-574.
- MONAGHAN, J.J., (2012), "Smoothed Particle Hydrodynamics and its diverse applications", *Ann. Rev. Fluid Mech.*, **44**, 323-346.
- MONAGHAN, J.J. and GINGOLD, R.A. (1983), "Shock simulation by the particle method SPH", *J. Comput. Phys.*, **52**, 374-389.
- PEREIRA, G.G. PRAKASH, M. and CLEARY, P.W., (2012), "SPH modelling of fluid at the grain level in a porous medium", *Appl. Math. Model.*, **35**, 1666-1675.
- TARTAKOVSKY, A.M., TRASK, N., PAN, K., JONES, B., PAN, W. and WILLIAMS, J.R., (2015), "Smoothed Particle Hydrodynamics and its applications for multiphase flow and reactive transport in porous media", *Comput. Geosci.*, DOI 10.1007/s10596-015-9468-9